Phase transitions in a continuum model of the classical Heisenberg magnet: The ferromagnetic system

Enrique Lomba
Instituto de Química Física Rocasolano, Consejo Superior de Investigaciones Científicas, Serrano 119, E-28006 Madrid, Spain

Jean-Jacques Weis
Laboratoire de Physique Théorique et Hautes Energies, Bâtiment 211, Université de Paris-Sud, 91405 Orsay Cedex, France

Noe G. Almarza and Fernando Bresme
Departamento de Química Física I, Universidad Complutense, E-28040 Madrid, Spain

George Stell*
Gruppe for Teoretisk Fysikk, Universitetet i Trondheim, N-7034 Trondheim-NTH, Norway
(Received 4 January 1994)

We present a detailed description of the rich variety of phase transitions exhibited by the continuum Heisenberg model of spin fluid, treated by means of integral equation methods (mean spherical approximation and reference hypernetted chain equation) and simulation techniques (canonical ensemble and Gibbs ensemble Monte Carlo). We focus here on ferromagnetic interactions. An order-disorder transition and a gas-liquid transition are characterized. Both transitions are coupled at low temperature, but near the gas-liquid critical point only ordered states are involved in the gas-liquid transition. Our data preclude the existence of a tricritical point, but there is evidence that the line of Curie points may end up in a critical end point at the gas-liquid spinodal. At low densities there is a strong tendency to clustering, and the system organizes in magnetized droplets. The reference hypernetted chain equation yields a spinodal line (locus of Curie points) for moderate to high densities, whereas at low densities the equation breaks down at a singularity with the characteristic behavior of a square root branch point.

PACS number(s): 61.20.Gy, 64.60.Cn, 71.10.+x

I. INTRODUCTION

The need to extend the well developed studies of magnetic lattice models to continuum disordered systems can be understood in terms of the great variety of physical properties connected to the lack of translational order, that can only be strictly accounted for in the context of liquid state theory. Such is the case of the effects associated with gas-liquid transitions (which as we will see might be coupled with changes in the magnetic ordering as well) or phenomena such as magnetostriction, absent by definition in rigid lattice models. Moreover, since the late 1960s there have been reports on the existence of liquid ferromagnetic materials, such as the Au-Co alloy studied by Bush and Guentherodt [1] and further confirmed by Kraeft and Alexander [2].

In this regard, disordered systems with interparticle spin interactions of classical Heisenberg symmetry have been studied in the past within the framework of classical statistical mechanics, in particular, by means of analytical approaches like the mean spherical approximation (MSA) [3–5] or mean fieldlike treatments [6,7]. A fundamental drawback in the use of the MSA lies on the fact that orientational and spatial contributions to the pair correlations are fully decoupled, to the point that the spatial distribution reduces to that of the hard-sphere fluid. Thereby, an MSA treatment will very likely be more suitable for spinglass systems (in which the spatial degrees of freedom are frozen and, therefore, decoupled from the orientational ones) than in the fully annealed spin fluid system. A nonlinear approach is thus required for a better theoretical description of the Heisenberg spin fluid. Recently, a two dimensional quantum spin fluid has also been studied in detail by path-integral Monte Carlo simulation and in a mean field approach by Marx, Nielaba and Binder [8].

The aim of this work is to explore the phase transitions that occur in a particularly simple model of disordered magnetic material, the classical Heisenberg model to a level of approximation far beyond the MSA. We will concentrate on the ferromagnetic system and in a forthcoming paper [9] a detailed analysis of the transitions undergone by the antiferromagnetic Heisenberg fluid will be presented. On one hand, we resort to an integral equation which has proven to yield excellent results in other nonspherically symmetric fluid systems, namely, the reference hypernetted chain (RHNC) [10,11] and on the other to computer simulations, using two complementary techniques, canonical ensemble and Gibbs ensemble (GEMC)

*Permanent address: Department of Chemistry, State University of New York at Stony Brook, Stony Brook, New York 11794-3400.

Monte Carlo [12]. The combined use of theoretical tools like the RHNC and MSA equations and computer simulation will furnish information on the location of spinodal decomposition lines and phase coexistence boundaries, as well as details on particle association at low temperatures and the configurational structure adopted by the fluid when crossing the instability boundaries.

The model Hamiltonian considered in this work is the simplest natural choice for a Heisenberg magnet, hard spheres of diameter σ with embedded Heisenberg spins, whose coupling constant is given by a Yukawa interaction

$$\beta u(12) = \begin{cases} \infty , & r < \sigma \\ \beta J(r)\Phi^{110}(12) , & r \geq \sigma , \end{cases} \tag{1.1}$$

with

$$\beta J(r) = -3K\frac{e^{-z(r-\sigma)}}{r} \tag{1.2}$$

and the rotational invariant $\Phi^{110}(12) = \mathbf{s}_1 \cdot \mathbf{s}_2$, $\mathbf{s}_i$ being the unit vector describing the orientation of the spin in particle i.

With the interaction so defined, $K > 0$ describes a system where parallel configurations are favored (ferromagnetic), whereas $K < 0$ implies favored antiparallel configuration (antiferromagnetic). There is an essential qualitative difference between the antiferromagnetic Heisenberg interaction and the dipole-dipole potential (although both favor antiparallel configurations) and is connected with the fact that this latter interaction favors head-to-tail (i.e., parallel) configurations as well, and, therefore, dipolar systems might exhibit both ferroelectric and antiferroelectric transitions [13]. Obviously, a Heisenberg antiferromagnet will never undergo a ferromagnetic transition. The screening parameter z determines the range of the interaction. In this work all computer simulation and RHNC results presented correspond to $z\sigma = 1$.

The structure of this work can be outlined as follows. The next section will deal with the symmetry properties of the Heisenberg interaction and its implications in the particular formulation of the Ornstein-Zernike (OZ) equation and, consequently, the RHNC theory. We also include here explicit expressions for the calculation of the thermodynamic properties. In Sec. III we recall some of the leading results of the MSA analytic solution and its application to the determination of spinodal lines. Relevant details regarding the use of Gibbs ensemble simulation in systems with spin interactions can be found in Sec. IV. Explicit results for the order-disorder and gas-liquid transitions are found in Sec. V, where we also pay attention to the singular behavior of the RHNC equation in the boundaries of its nonsolution region. Finally, an appendix with some numerical subtleties essential in an efficient solution of the RHNC equation for systems with Heisenberg spin interactions is also included. In particular, we introduce an extension of a hybrid Newton-Raphson algorithm [14] adequate for systems with angular-dependent functions, with considerable simplifications derived from the peculiar symmetry of the spin-spin interaction.

II. SYMMETRY PROPERTIES OF THE HEISENBERG INTERACTION. RHNC EQUATIONS FOR THE SPIN FLUID

A. Interaction symmetry and averaged low density limit of the pair distribution function

With the intermolecular potential described by Eq. (1.1) one immediately notices that the correlation functions must have a particularly simple orientational dependence, since the rotational invariant Φ^{110} is independent of $\mathbf{r}_{12}$, the vector joining the centers of particles 1 and 2. This also implies that the angular averages of the potential are extraordinarily simple. First, one has $\langle u(12)\rangle_{\omega_1\omega_2} = 0$, a feature common with all multipolar interactions. But here we have, in addition

$$\langle u(12)\rangle_{\omega_1} = \langle u(12)\rangle_{\omega_2} = 0 . \tag{2.1}$$

In general the average of all odd powers of $u(12)$ will vanish. For even powers we will have a simple expression

$$\langle u(12)^{2k}\rangle_{\omega_1\omega_2} = \frac{J(r)^{2k}}{2k+1} . \tag{2.2}$$

With this it can be shown that the radial component of the low density limit of the pair distribution function, $g(12)$, is simply

$$\lim_{\rho\to 0} g_{000}(r) = \langle \exp[-\beta u(12)]\rangle_{\omega_1\omega_2} = \frac{\sinh \beta J(r)}{\beta J(r)} . \tag{2.3}$$

An angular averaged interaction (or average potential of mean force) can be defined by

$$\beta u_{av}(r) = -\ln\frac{\sinh \beta J(r)}{\beta J(r)} , \tag{2.4}$$

which implies that, whatever the sign of the coupling constant, there will be a net attraction between particles, and, thus, gas-liquid condensation might occur for sufficiently low temperatures, as long as the range of the interaction is sufficiently large [15,16].

B. The OZ relation and RHNC closure

The aforementioned properties of the interaction imply that the expansion of the total correlation function, $h(12)$, in rotational invariants [17] [and the same applies to the direct correlation function, $c(12)$] contains only the subset of $h^{mnl}(r)$ coefficients with $l = 0$, and since $|m-n| \leq l \leq m+n$, one has the additional restriction $m = n$. Hence

$$h(12) = \sum_l h^{ll0}(r)\Phi^{ll0}(12) . \tag{2.5}$$

Moreover, the relation between these h^{mnl} coefficients and those of the spherical harmonic expansion in the axial reference frame (in which the z axis joins the molec-

ular centers) is straightforward

$$h_{ll m}(r) = \frac{1}{2l+1}(-1)^m h^{ll0}(r) \ . \tag{2.6}$$

This alternative expansion is especially useful since for potentials with axial symmetry the OZ equation in Fourier space decouples into a linear matrix equation [11]. Hereafter, we will only refer to axial (lower indices) coefficients. In Fourier space the OZ relation reads

$$\tilde{h}(k,\omega_1,\omega_2) = \tilde{c}(k,\omega_1,\omega_2) + \rho \int \tilde{c}(k,\omega_1,\omega_3)\tilde{h}(k,\omega_3,\omega_2)d\omega_3 \ , \tag{2.7}$$

which, by using the axial spherical harmonic expansion, in our case decouples into

$$\tilde{h}_{ll m}(k) = \tilde{c}_{ll m}(k) + (-1)^m \rho \tilde{c}_{ll m}(k)\tilde{h}_{ll m}(k) \ . \tag{2.8}$$

Because of Eq.(2.6) the only relevant equations correspond to $m = 0$. Note that in this particular case the $\tilde{f}_{ll0}(k)$ transforms are evaluated by standard three-dimensional Fourier transformation of $f_{ll0}(r)$ and the cumbersome higher order Hankel transforms [11] can be avoided.

The RHNC closure relation now reads

$$c_{ll0}(r) = -\delta_{l0} - \gamma_{ll0}(r) + \Big\langle \exp[-\beta u(12) + 4\pi \sum_{n,m} \gamma_{nn0}(r) Y_{nm}(\omega_1) Y_{l\bar{m}}(\omega_2) + B_0(r)] | ll0 \Big\rangle \ , \tag{2.9}$$

where $\gamma_{ll0}(r) = h_{ll0}(r) - c_{ll0}(r)$ and $\langle \cdots | ll0 \rangle$ denotes the projection onto the angular function $Y_{l0}(\omega_1)Y_{l0}(\omega_2)$. The function $B_0(r)$ is the bridge function of a reference system, for which in this work we have used the hard-sphere fluid, described using parametized expressions for $g(r)$ and the background function, $y(r)$ [18]. The hard-sphere diameter is chosen so that the free energy of the system is minimized, according to the optimization criterion proposed by Lado, Foiles, and Ashcroft [10], which reduces to finding the hard-sphere diameter σ_{ref} which fulfills

$$\int_0^\infty r^2 \left[g_{000}(r) - g_0(r;\sigma_{ref})\right] \frac{\partial B_0(r;\sigma_{ref})}{\partial \sigma_{ref}} dr = 0 \ . \tag{2.10}$$

Equation (2.9) coupled with the OZ relation

$$\tilde{\gamma}_{ll0}(k) = \frac{\rho \tilde{c}_{ll0}(k)^2}{1 - \rho \tilde{c}_{ll0}(k)} \ , \tag{2.11}$$

constitute the RHNC approximation for the Heisenberg spin fluid. We have solved this highly nonlinear set of coupled equations using a hybrid Newton-Raphson procedure [14] extended to systems with noncentral forces (see Ref. [19] for a method similar in scope applied to dipolar hard spheres). Some technical details can be found in the Appendix.

A key feature in the RHNC approximation is that one can have a full description of the thermodynamics in terms of the correlation functions, i.e., thermodynamic integration can be performed explicitly over the closure relation leading to simple explicit expressions for the thermodynamic potentials. This desirable feature, shared by MSA and HNC, is absent from other approximations like the hybrid MSA (HMSA) or the crossover integral equation [20,21]. The excess internal energy simply reads

$$\beta U/N = -6\pi\rho K e^{z\sigma} \int_\sigma^\infty h_{110}(r) r e^{-zr} dr \tag{2.12}$$

and the virial equation

$$\beta P/\rho = 1 - \frac{2\pi}{3}\rho\sigma^3 g_{000}(\sigma^+) - 2\pi\rho K e^{z\sigma} \int_\sigma^\infty h_{110}(r)(zr+1) r e^{-zr} dr \ . \tag{2.13}$$

Finally, the excess free energy in the RHNC approximation is given by

$$\beta A^{ex}/N = 2\pi\rho \int_{\sigma_{ref}}^\infty g_0(r) B_0(r) r^2 dr \times \frac{1}{4\pi^2\rho} \int_0^\infty k^2 \sum_l (2l+1) \Big\{ \ln[1 + \rho\tilde{h}_{ll0}(k)] - \rho\tilde{h}_{ll0}(k) + \rho^2 \tilde{h}_{ll0}(k) \times \Big(\frac{1}{2}\tilde{h}_{ll0}(k) - \tilde{\gamma}_{ll0}(k) \Big) \Big\} dk - \frac{1}{2\rho}\tilde{c}_{000}(0) \ . \tag{2.14}$$

Here the so-called "universality" principle of the bridge function [10] is understood, which despite its limited validity [22], in this particular case leads to expressions whose thermodynamic consistency is remarkable.

Other quantities of interest are the inverse isothermal compressibility

$$\chi_{000}^{-1} = 1 - 4\pi\rho \int_0^\infty r^2 c_{000}(r) dr \tag{2.15}$$

and inverse isothermal magnetic susceptibility

$$\chi_{110}^{-1} = 1 - 4\pi\rho \int_0^\infty r^2 c_{110}(r) dr \tag{2.16}$$

quantities that should vanish at the gas-liquid spinodal and at the Curie point, respectively. In the paramagnetic-antiferromagnetic transition, the corresponding Néel point is characterized by a singularity in $\rho\chi_{110}/\beta$ associated with a finite discontinuity in its derivatives (but the susceptibility remains finite when the system undergoes the transition [23]) and a zero in

$$\chi_{220}^{-1} = 1 - 4\pi\rho \int_0^\infty r^2 c_{220}(r) dr \ . \tag{2.17}$$

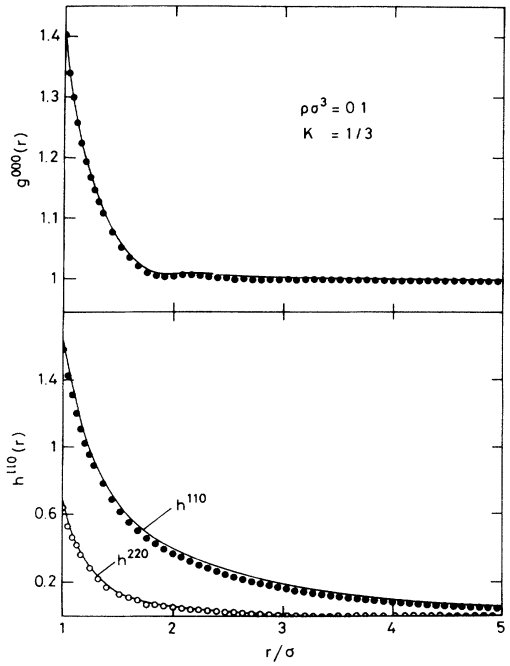

FIG. 1. $g^{000}(r)$ and $h^{110}(r)$ components of the total correlation function for the Heisenberg ferrofluid at low density ($\rho\sigma^3 = 0.1$ and $T^* = 3$). MC simulation (symbols) vs RHNC (lines).

These orientational quantities are closely connected with the inverse of the G_1 and G_2 Kirkwood parameters, which in dielectric media are related with the permitivity and Kerr constant, respectively [24].

Figures 1 and 2 illustrate the accuracy of the RHNC approximation for the determination of the correlation

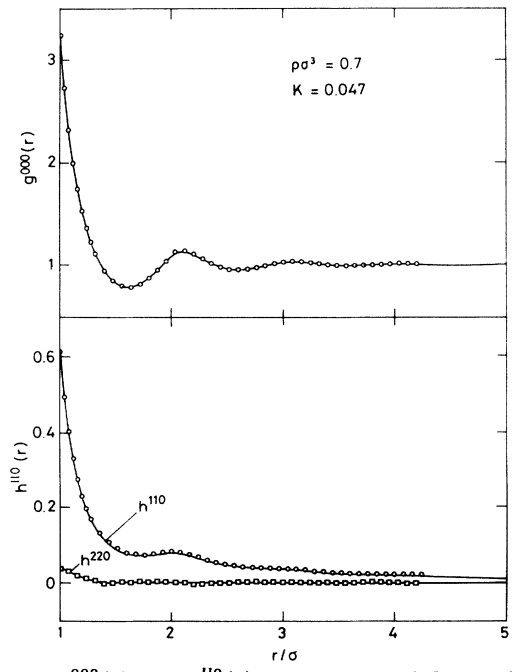

FIG. 2. $g^{000}(r)$ and $h^{110}(r)$ components of the total correlation function for the Heisenberg ferrofluid at high density ($\rho\sigma^3 = 0.7$ and $T^* = 21.3$). MC simulation (symbols) vs RHNC (lines).

TABLE I. RHNC vs MC results for a Heisenberg ferrofluid.

$\rho\sigma^3$	T^*	$\beta U/N$		$\beta P/\rho$	
		MC	RHNC	MC	RHNC
0.7	21.43	-0.040	-0.039	5.64	5.69
0.1	3.33	-0.135	-0.140	1.14	1.20

functions of the Heisenberg ferrofluid. In both the low and high density calculations the agreement between theory and simulation (described in Sec. V) is almost perfect. This is complemented by some results for the thermodynamic properties presented in Table I.

III. MEAN SPHERICAL APPROXIMATION. AN ANALYTIC APPROACH

The solution of the MSA for systems with interaction potentials described by Eq. (1.1) was found some time ago by Høye and Stell [3]. They reduced the angular-dependent integral equation to a simple one-component Yukawa problem [25] with a peculiar core condition [26] ($h^{110} = 0$ inside the core). After tedious algebraic manipulation it all reduces to finding the roots of the equation

$$u_0^3 + u_1^2 - \frac{1}{4}z^2 u_0 = 0 \ , \tag{3.1}$$

with

$$u_0 = 6\xi K(1 - \omega v/K)^2 \ ,$$
$$u_1 = -3\xi K(1 - \omega v/K)(1 - \gamma v/K) \ ,$$

where $\omega = (e^{-z} - 1)/2z$, $\gamma = (e^{-z} + 1)/2z$, and $\xi = \pi\rho\sigma^3/6$. The parameter v fully determines the MSA solution and is related to the excess internal energy

$$\beta U^{ex}/N = -\frac{3}{2}v(\xi, K). \tag{3.2}$$

When the interactions are ferromagnetic the MSA solution presents a Curie line when $u_0 = (-1+\sqrt{1+z^2})/2$. By using Eqs. (16), (17), and (21) of Ref. [3] it is easy to determine the locus of Curie points in the $K-\xi$ plane (or more naturally $T^* - \xi$ with $T^* = 1/|K|$). Together with the spinodal line, the MSA for the one Yukawa problem exhibits a nonsolution line [4] which is defined by the equation

$$\mathcal{D}\left[u_0^3 + u_1^2 - \frac{1}{4}z^2 u_0\right] = 0 \ , \tag{3.3}$$

where $\mathcal{D}$ refers to the discriminant of the algebraic equation. Thus, Eq. (3.3) determines the onset of complex solutions in the MSA. In Fig. 3 we show the MSA spinodal and nonsolution lines for the ferromagnetic interactions. We see that for low z the no-solution line is squeezed against the spinodal and they are hardly distinguishable. As z increases the difference is more apparent. A determination of the gas-liquid transition using MSA thermodynamics (as was done by Rushbrooke,

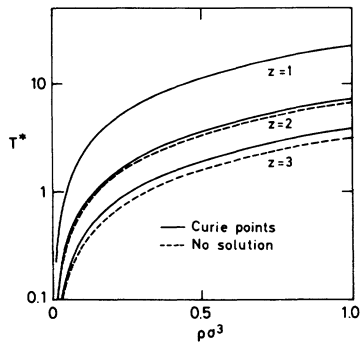

FIG. 3. Curie and nonsolution lines in the MSA for a Heisenberg ferrofluid with varying Yukawa screening parameters [see Eq. (1.2)].

Stell, and Høye for the dipolar hard-sphere fluid [27]) is prevented by the location of the complex solution region in the $T^* - \xi$ diagram. On the contrary, for antiferromagnetic interactions, where by construction there is no antiferromagnetic transition in the MSA (since it is associated with the coefficients h_{220} which are neglected), it will be possible to predict a gas-liquid transition from the MSA internal energy route to thermodynamics [9].

IV. GIBBS ENSEMBLE SIMULATION IN THE SPIN FLUID

The GEMC method [28] facilitates the investigation of equilibrium between two phases by simulating two subsystems that do not have energy interactions between them, but exchange volume and particles. Total volume and total number of particles are constant but the values in the subsystems change so that mechanical and chemical equilibria conditions are fulfilled.

We have carried out GEMC simulations to investigate the liquid-gas coexistence curve of our spin fluid, using two cubic boxes with periodic boundary conditions. In each box the interaction potential was truncated at half the box length $L/2$. A long range correction to the internal energy was obtained by estimating the interaction energy of one particle with the particles beyond the cutoff distance through

$$U_{LR}(\mathbf{s}_i) = N\mathbf{s}_i \cdot \frac{\mathbf{M}}{N}\lambda(L) \ , \tag{4.1}$$

where

$$\lambda(L) = \frac{1}{L^3}\int_{L/2}^{\infty} J(r)d\mathbf{r} \ . \tag{4.2}$$

The approximation (4.1) amounts to assure that the particles beyond $L/2$ are distributed uniformly with orientation $\mathbf{M}/N$ independent of position, where

$$\mathbf{M} = \sum_{k=1}^{N} \mathbf{s}_k \ . \tag{4.3}$$

The long range correction to the total energy is then given by

$$U_{LR} = \frac{1}{2}\lambda(L)M^2 \ . \tag{4.4}$$

In the GEMC method three types of MC moves are required: displacements of particles within the subsystems, volume changes of the two subsystems (in such a way that the total volume remains constant) and exchange of particles between subsystems. These three steps were performed following the procedure described in Ref. [28]. However, the efficiency of the simulations were improved by using a biasing scheme for sampling orientational coordinates [29].

The interaction energy of a particle i with the other particles of the simulation box is given by

$$u_i = \sum_{j\neq i} u_{hs}(r_{ij}) + \mathbf{s}_i \cdot \sum_{j\neq i} J(r_{ij})H(L/2 - r_{ij})\mathbf{s}_j + \lambda(L)\mathbf{s}_i \cdot \mathbf{M} \ , \tag{4.5}$$

where u_{hs} is the hard-sphere potential, $H(x)$ is the step function, and a long range correction term has been included. If the particle i does not overlap with any other particle, Eq. (4.5) can be written in the form

$$u_i = \mathbf{s}_i \cdot \mathbf{W}_{id} + \lambda(L) \ , \tag{4.6}$$

where

$$\mathbf{W}_{id} = \mathbf{s}_i \cdot \sum_{j\neq i} J(r_{ij})H(L/2 - r_{ij})\mathbf{s}_j + \lambda(L)\sum_{j\neq i}\mathbf{s}_j \tag{4.7}$$

depends on positions and orientations of the rest of the particles in the subsystem as well as on the position of particle i but not on its orientation.

Suppose we have generated a *trial* position for the particle i, and this position is not rejected due to the hard-sphere interactions between particles. Then we choose a new orientation of the normalized $\mathbf{s}_i$ vector according to the modulus and orientation of $\mathbf{W}_{id}$.

The new vector $\mathbf{s}_i$ is chosen with probability given by

$$\alpha(\mathbf{s}_i) = \frac{\exp[-\beta(\mathbf{W}_{id}\cdot\mathbf{s}_i)]}{\int \exp[-\beta(\mathbf{W}_{id}\cdot\mathbf{s}_i)]\,d\mathbf{s}_i} \ , \tag{4.8}$$

which by integration leads to

$$\alpha(\mathbf{s}_i) = \frac{\exp[-\beta(\mathbf{W}_{id}\cdot\mathbf{s}_i)]}{Z(|\,\mathbf{W}_{id}\,|)} \ , \tag{4.9}$$

where

$$Z(|\,\mathbf{W}_{id}\,|) = \frac{4\pi}{\beta\,|\,\mathbf{W}_{id}\,|}\sinh(\beta\,|\,\mathbf{W}_{id}\,|) \ . \tag{4.10}$$

According to detailed balance prescription [30] in a translational (and rotational) move of a particle without change of box, the acceptance probabilities, A, should fulfill

$$\frac{A(\mathbf{r}_i^n,\mathbf{s}_i^n \mid \mathbf{r}_i^o,\mathbf{s}_i^o)}{A(\mathbf{r}_i^o,\mathbf{s}_i^o \mid \mathbf{r}_i^n,\mathbf{s}_i^n)} = \frac{\alpha(\mathbf{r}_i^o,\mathbf{s}_i^o \mid \mathbf{r}_i^n,\mathbf{s}_i^n)}{\alpha(\mathbf{r}_i^n,\mathbf{s}_i^n \mid \mathbf{r}_i^o,\mathbf{s}_i^o)}\frac{\exp[-\beta(\mathbf{W}_{id}^n\cdot\mathbf{s}_i^n)]}{\exp[-\beta(\mathbf{W}_{id}^o\cdot\mathbf{s}_i^o)]} = \frac{Z(W_{id}^n)}{Z(W_{id}^o)} \ . \tag{4.11}$$

TABLE II. Technical details of the GEMC simulations. N=216, $V/\sigma^3 = 540$, $N^{eq}_{cycles}/10^3 = 100$, $N^{ave}_{cycles}/10^3 = 200$, $N_t = 216$, $N_{ch} = 1080$ (except columns F and G for which $N_{ch} = 432$ and 216, respectively).

Case	A	B	C	D	E	F	G
T^*	4.485	4.689	4.893	5.097	5.301	5.505	5.709
$\rho_g\sigma^3$	0.104(6)	0.131(7)	0.153(8)	0.175(30)	0.208(28)	0.216(11)	0.253(8)
$\rho_l\sigma^3$	0.782(6)	0.756(8)	0.724(8)	0.683(9)	0.641(17)	0.590(11)	0.539(7)
$\langle\beta U/N\rangle_g$	-0.10(1)	-0.14(3)	-0.19(4)	-0.21(4)	-0.45(2)	-0.44(1)	-0.79(1)
$\langle\beta U/N\rangle_l$	-6.66(7)	-6.09(8)	-5.51(9)	-4.86(8)	-4.19(1)	-3.71(1)	-3.05(1)
$\langle\beta p\sigma^3\rangle_g$	0.12(1)	0.15(1)	0.18(1)	0.20(1)	0.22(1)	0.24(1)	0.25(1)
$\langle\beta p\sigma^3\rangle_l$	0.15(7)	0.22(9)	0.18(6)	0.17(5)	0.19(6)	0.20(4)	0.21(3)
$\langle M^2/N^2\rangle_g$	0.082(1)	0.094(9)	0.11(2)	0.124(15)	0.24(12)	0.24(5)	0.36(2)
$\langle M^2/N^2\rangle_l$	0.902(1)	0.893(1)	0.882(2)	0.867(2)	0.849(4)	0.826(6)	0.786(6)
A_g	6.6(4)	4.8(4)	3.8(3)	3.4(2)	2.8(2)	2.5(1)	2.19(3)
$\beta\mu_g - \ln\Lambda^3$	-1.90(6)	-1.57(8)	-1.32(9)	-1.21(7)	-1.05(8)	-0.91(4)	-0.78(2)
A_l	6.8(7)	4.7(5)	3.7(4)	3.3(2)	2.8(3)	2.5(1)	2.17(3)
$\beta\mu_l - \ln\Lambda^3$	-1.92(10)	-1.56(10)	-1.32(10)	-1.20(7)	-1.05(9)	-0.90(5)	-0.78(2)

Such a relationship is satisfied with the acceptance probability given by

$$A\left(\mathbf{r}_i^n, \mathbf{s}_i^n \mid \mathbf{r}_i^o, \mathbf{s}_i^o\right) = \min\left[1, \frac{Z\left(W_{id}^n\right)}{Z\left(W_{id}^o\right)}\right] . \tag{4.12}$$

When particle exchange is attempted, we first choose at random the box from which a particle will be removed and try to insert it into the other box in a position chosen at random. If there is no overlap, the orientation of the inserted spin is chosen with probability (4.9) as before. In this step the acceptance probability, satisfying detailed balance, is

$$A\left(\mathbf{r}_i^n, \mathbf{s}_i^n; i \in b \mid \mathbf{r}_i^o, \mathbf{s}_i^o; i \in a\right)$$

$$= \min\left[1, \frac{V_b}{V_a}\frac{Z\left(W_{id}^n\right)}{Z\left(W_{id}^o\right)}\frac{n_a}{n_b+1}\right] . \tag{4.13}$$

The liquid-vapor equilibria of the Heisenberg ferromagnet were simulated for several temperatures with a total number of 216 particles. Simulation runs were organized in cycles, a cycle consisting of N_t trial displacement moves, N_{ch} trial interchanges of particles and one trial change of volume. Technical details of the runs, as well as results for thermodynamic properties are summarized in Table II.

V. SPINODAL LINES AND PHASE COEXISTENCE

Figure 4 shows the Curie lines obtained from the MSA and RHNC equations together with the gas-liquid coexistence curve determined from the GEMC calculations. An immediate observation is that the gas-liquid coexistence lies for the most part below the line of Curie points. The MSA and RHNC approximations give fairly consistent results. However, whereas MSA yields a true spinodal for all densities this is so for the RHNC equation only at densities $\rho\sigma^3 > 0.2$. At lower densities a qualitatively different behavior occurs in which the magnetic susceptibility remains finite but presents a square root branch point singularity, indicating the onset of complex solutions (and breakdown of the real numerical solution). Similar behavior is known to exist in other systems for approximations like the HNC or Percus-Yevick equations. Following ideas of Belloni [31], we have investigated a nonlinear fit of both compressibility and susceptibility to

$$\chi_{ll0}^{-1} = a\sqrt{T^* - T_s^*} + b , \tag{5.1}$$

where $T^* = 1/K$. The results, for $\rho\sigma^3 = 0.01$, are shown in Fig. 5, which plots the difference

$$\Delta = \chi_{ll0}^{-1} - \chi_{ll0_s}^{-1} , \tag{5.2}$$

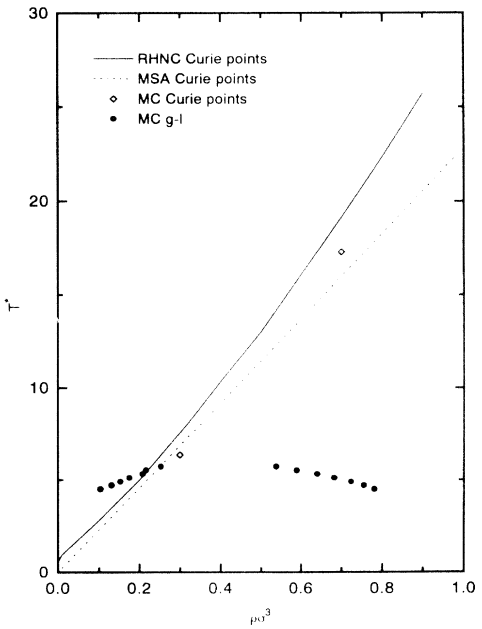

FIG. 4. Locus of Curie points and no-solution line in the RHNC approximation (solid line) and MSA spinodal (dashed line) vs MC estimates (diamonds). Gibbs ensemble estimates of the gas-liquid coexistence are represented by solid circles.

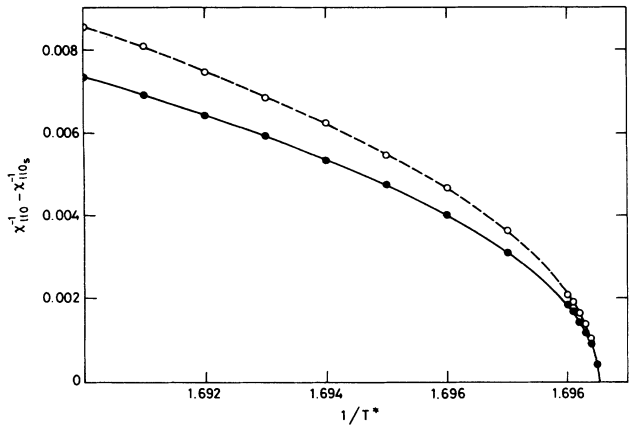

FIG. 5. Variation of the inverse isothermal compressibility and magnetic susceptibility (lower and upper curve, respectively) in the vicinity of the nonsolution line at low density ($\rho\sigma^3 = 0.01$). RHNC results are denoted by circles and lines correspond to a nonlinear fit to Eq. (5.1).

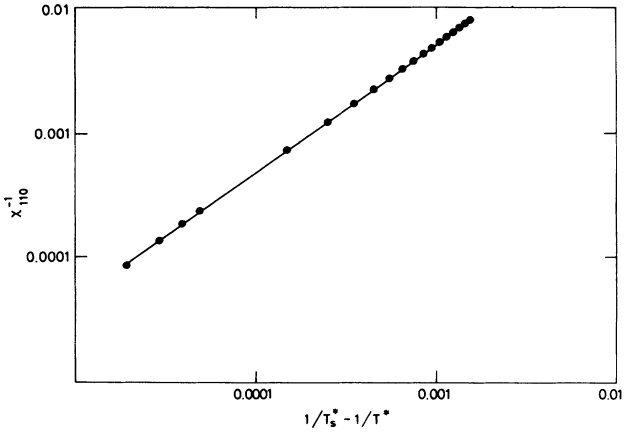

FIG. 6. Inverse isothermal magnetic susceptibility in the vicinity of the Curie temperature at moderate density ($\rho\sigma^3 = 0.3$). RHNC results are denoted by solid circles and the lines correspond to a nonlinear fit to Eq. (5.3).

where the subscript s denotes the value computed for T_s^*. (The RHNC values are represented by circles and the results of the fit by a solid line.) A striking result is that the singular point is the same for both compressibility and magnetic susceptibilities. For the density considered it corresponds to $K_s = 1.68953 \pm 0.000005$. Great care has been taken to obtain accurate results. The RHNC equation was solved using a mesh of 16 384 grid points spaced by $\Delta r = 0.01\sigma$. Reducing the number of points by half hardly changed the location of the singular point. For $\rho\sigma^3 > 0.2$ a fit to Eq. (5.1) is no longer possible. Instead the magnetic susceptibility (but not the isothermal compressibility) follows a power law

$$\chi_{110}^{-1} = a(T^* - T_{s_1}^*)^{\gamma} , \tag{5.3}$$

in the vicinity of the nonsolution boundary with critical exponent $\gamma \approx 1$, close to the classical value. The variation of χ_{110}^{-1} as a function of temperature is shown in Fig. 6 (log-log plot) for $\rho\sigma^3 = 0.3$ ($\gamma = 1.008 \pm 0.0005$). The divergence of χ_{110} is accompanied by a corresponding divergence in χ_{220} reflecting preferential parallel (nematic) ordering of the spins. In antiferromagnetic systems only χ_{220} diverges.

It might be possible that the failure of the RHNC equation to capture the low density spinodal behavior is connected with the inability of the equation to account for clustering, which is important in low density systems with strong attractive interactions. A similar speculation has been put forward to explain related phenomena in the restricted primitive model of electrolytes [32]. In the MSA approximation (which does not reproduce clustering effects correctly either) the boundary of complex solutions always lies inside the spinodal [33]. Approximations that retain the structure of MSA at low densities (as, for instance, the crossover integral equation [21]) might be able to reproduce the spinodal behavior at low densities [34] even if the treatment of association effects is poor.

An attempt has been made to compare the Curie temperatures predicted by the RHNC and MSA approximations with estimates obtained from MC simulations. Towards this end we calculated the temperature dependence of the magnetization $M = \langle\sqrt{M^2}/N\rangle$ of a system of 500 particles in a cubic box with periodic boundary conditions. Averages were taken over runs involving generally of the order of 10 000–20 000 trial moves per particle after equilibration. These are shown in Fig. 7 for two different densities. As expected from extensive MC calculations of the lattice version of the classical Heisenberg ferromagnet (with nearest neighbor interactions) the magnetization curves show appreciable rounding effects near the critical temperature due to the finite size of the system [35], which preclude an accurate determination of the Curie temperature. For the lattice systems these difficulties have largely been overcome by applying finite-size scal-

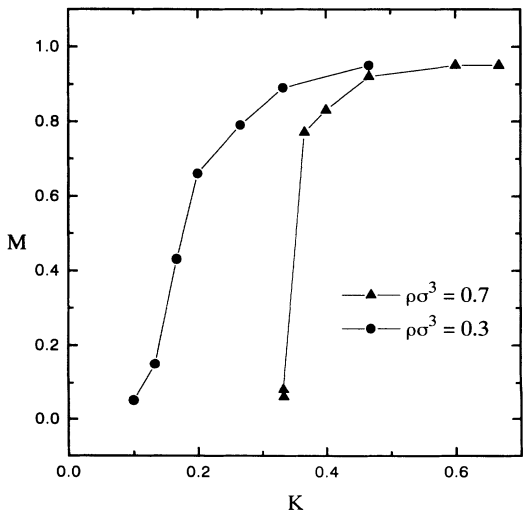

FIG. 7. Magnetization curves for a system of 500 particles in a cubic box with periodic boundary conditions from MC simulations.

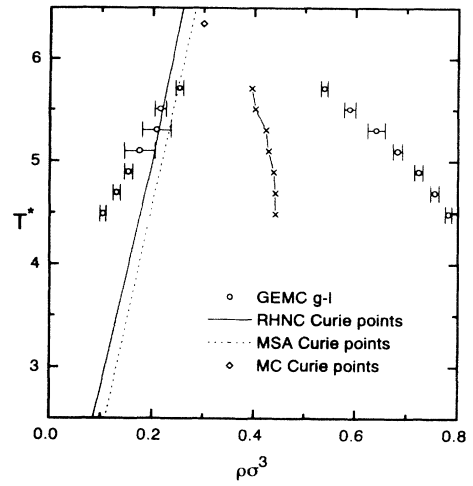

FIG. 8. Gas-liquid phase coexistence obtained from GEMC simulations.

ing concepts. [For the most refined lattice calculations of the three-dimensional (3D) Heisenberg model see Ref. [36].] Such a computationally expensive analysis seemed however, out of scope at the present stage of investigation of the off-lattice system. A rough estimate of the Curie temperature was obtained by assigning it to the temperature for which $M \sim 0.5$ (see Ref. [35]). The values so obtained compare favorably with both the RHNC and MSA results (cf. Fig. 4) but are clearly not accurate enough to assess the superiority of one theory over the other.

Results for the gas-liquid coexistence estimated through Gibbs ensemble simulation are shown in Fig. 4 and in more detail in Fig. 8. As mentioned before, this transition cannot be analyzed by the integral equation methods since it lies inside the nonsolution boundary (i.e., inside the line of Curie points and/or the boundary of complex solutions in the MSA). The fact that the gas phase is mainly paramagnetic and the liquid phase is ferromagnetic, except in the neighborhood of the critical point, implies that both transitions will mostly be coupled. The system will, however, lack a tricritical point and the line of Curie points will end up at the gas-liquid spinodal in a critical end point. The Heisenberg spin fluid phase diagram is qualitatively similar to that of the two-dimensional quantum case studied by Marx *et al.* [8], but there a tricritical point is present. In our case, we see that the upper part of the gas-liquid coexistence curve is below the magnetic spinodal, and the equilibrium takes place between orientationally ordered ferromagnetic states. The error bars near the order-disorder transition indicate large density fluctuations associated with large energy fluctuations. This can be easily understood given the proximity of the Curie point.

Snapshots of configurations obtained from the MC simulations are shown in Figs. 9–13. Inside the two-phase region, at densities $\rho\sigma^3 = 0.1$ (Figs. 9 and 10) and $\rho\sigma^3 = 0.3$ (Fig. 11) one observes equilibrium coexistence between magnetized liquid drops and gas. The organization of the spins at high density ($\rho\sigma^3 = 0.7$) below and above the Curie temperature (ferromagnetic and paramagnetic phases, respectively) is shown in Figs. 12 and 13.

ACKNOWLEDGMENTS

NAVF (Norske Almenvitenskapelige Forskningsråd) is acknowledged for the support provided to cover computer time expenses at the CRAY YMP in SINTEF (Trondheim, Norway). Acknowledgment is also made to the Cornell National Supercomputer Facility, a resource of Center for Theory and Simulations in Science and Engineering, which receives major funding from the National Science Foundation and IBM Corporation, with additional support from New York State and members of the Corporate Research Institute. We thank D. Levesque for useful discussion. E.L. would like to thank the CNRS for supporting his visit to the Laboratoire de Physique Théorique et Hautes Energies, Université de Paris–Sud. Part of this work has been financed by Spanish Dirección General de Investigación Científica y Técnica (DGICYT) under Grant No. PB91-0110. G.S. is indebted to the National Science Foundation for its support while at Stony Brook.

APPENDIX: NUMERICAL SOLUTION PROCEDURE

In what follows we briefly sketch the outline of the hybrid Newton-Raphson solution procedure for the spin fluid OZ equation. For simplicity we will use the following conventions when naming the functions involved in the numerical scheme : $C_l(r_i) = r_i c_{ll0}(r_i)$ and $\tilde{C}_l(k_j) = k_j \tilde{c}_{ll0}(r_j)$ with $r_i = i\Delta r$ and $k_j = j\Delta k$, $i, j = 1, \ldots, N$

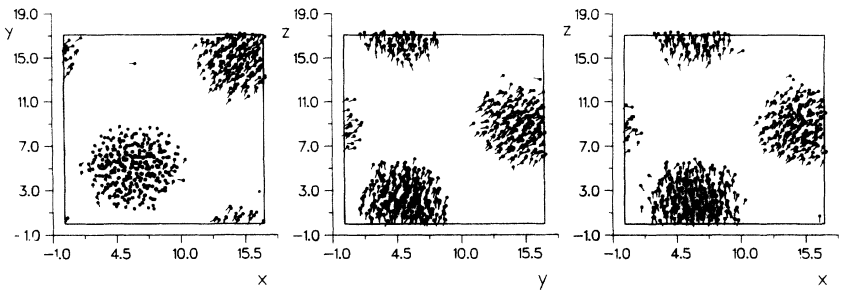

FIG. 9. Snapshot of a low density ferromagnetic fluid configuration of $\rho\sigma^3 = 0.1$ and $T^* = 1.875$. [Projection of the spins (500) on the xy, yz, and xz planes of the periodic simulation cell.] Distances are in units of σ.

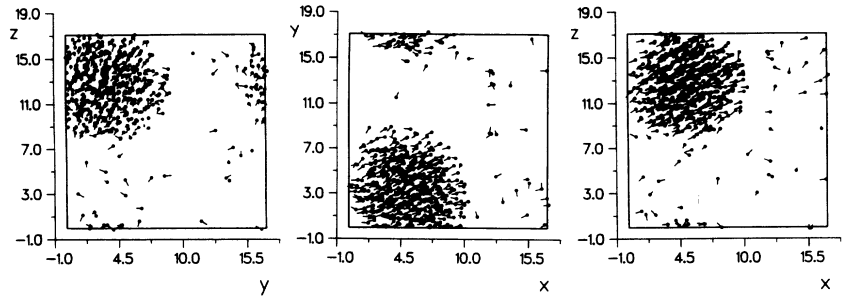

FIG. 10. Same as Fig. 9 but for $T^* = 2.7$ (temperature close to the Curie temperature).

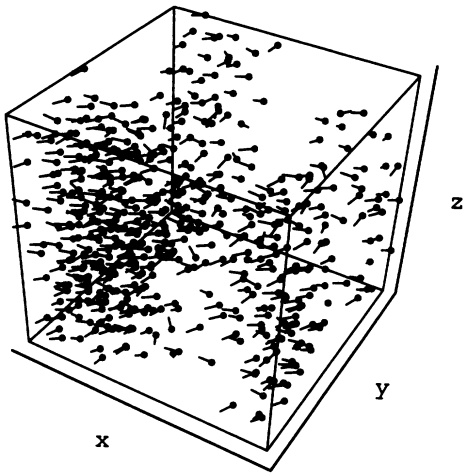

FIG. 11. 3D snapshots of a magnetized configuration at $\rho\sigma^3 = 0.3$ and $T^* = 3$. This thermodynamic state is inside the two-phase region.

and $\Delta r \Delta k = \pi/N$. $\Gamma_l(r_i)$ and $\tilde{\Gamma}_l(k_j)$ are similarly defined in terms of γ_{ll0}. With these definitions, the uncoupled OZ relations in Fourier space read

$$\Phi_l(k_j) = \tilde{\Gamma}_l(k_j) - \frac{\rho \tilde{C}_l(k_j)^2}{k_j - \rho \tilde{C}_l(k_j)} = 0 \tag{A1}$$

and the closure relations

$$C_l(r_i) = r_i \Big\langle \exp\Big(-\beta u(12) + \frac{1}{r} \sum_{\lambda} \Gamma_\lambda \phi^{\lambda\lambda 0}(12) - B_0(r) \Big) | ll0 \Big\rangle - r_i \delta_{l0} - \Gamma_l(r_i) \ . \tag{A2}$$

We can now proceed to expand the direct correlation function in k space in terms of the $\tilde{\Gamma}_l$ functions [37] around an initial estimate Γ_l^0,

$$\tilde{C}_l(k_j) = \tilde{C}_l^0(k_j) + \sum_{\lambda,i} \mathcal{C}_{l\lambda;ij} [\tilde{\Gamma}_\lambda(k_i) - \tilde{\Gamma}_\lambda^0(k_i)] \ , \tag{A3}$$

where

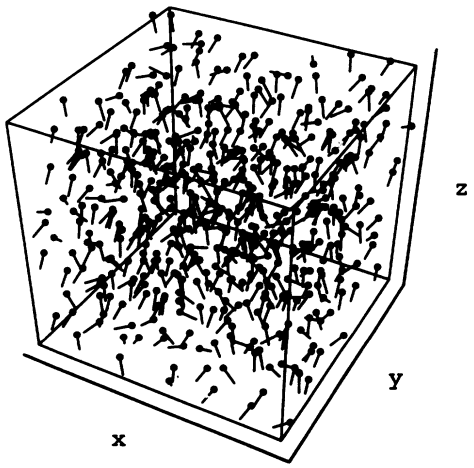

FIG. 12. 3D snapshots of a system of 500 spins at $\rho\sigma^3 = 0.7$ and $T^* = 10$ (ferromagnetic phase).

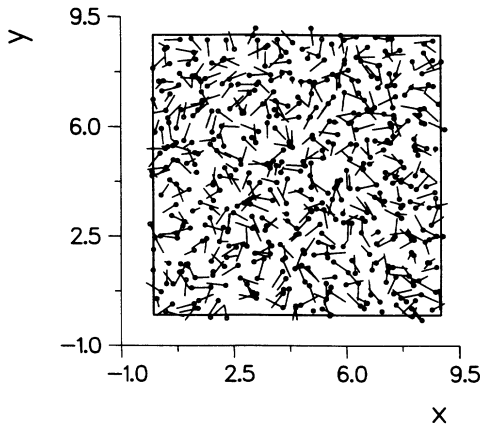

FIG. 13. Projection on the xy plane of the periodic simulation cell of an instantaneous configuration of 500 spins in the paramagnetic (orientationally disordered) fluid phase ($\rho\sigma^3 = 0.7$ and $T^* = 18.75$).

$$\mathcal{C}_{l\lambda;ij} = \frac{d\tilde{C}_l(k_j)}{d\tilde{\Gamma}_\lambda(k_i)} \ . \tag{A4}$$

This quantity can be shown to be equal to [37]

$$\mathcal{C}_{l\lambda;ij} = \frac{1}{N}\left[D_{l\lambda}(|i-j|) - D_{l\lambda}(i+j)\right] \ , \tag{A5}$$

with

$$D_{l\lambda}(n) = \sum_i \left(\frac{dC_l(r_i)}{d\Gamma_\lambda(r_i)}\right)_0 \cos \pi i n \ . \tag{A6}$$

From the closure relations (A2) one gets

$$\left(\frac{dC_l(r_i)}{d\Gamma_\lambda(r_i)}\right) = \left\langle \exp\left[-\beta u(12) + \frac{1}{r}\sum_{\lambda'}\Gamma_{\lambda'}\phi^{\lambda'\lambda'0}(12) - B_0(r)\right]\phi^{\lambda\lambda 0}(12)|ll0\right\rangle - \delta_{l\lambda} \ . \tag{A7}$$

Hence, if we use the expansion of Eq.(A3) for $j = 1,\ldots,M$ [with $0 < k < k_M$ representing the most significant region in k space as far as the structure of $\tilde{\Gamma}_l(k)$ is concerned], one can solve Eq. (A1) by Newton-Raphson iterations

$$\tilde{\Gamma}_l^{(n+1)}(k_j) = \tilde{\Gamma}_l^{(n)}(k_j) - \sum_{\lambda i}[\mathbf{J}^{-1}]_{l\lambda;ij}\tilde{\Phi}_\lambda(k_i) \ , \tag{A8}$$

where the Jacobian matrix elements can be computed by differentiation of Eq. (A1), to yield

$$[\mathbf{J}]_{l\lambda;ij} = \delta_{ij}\delta_{l\lambda} - \frac{\rho\tilde{C}_l(k_j)}{k_j - \rho\tilde{C}_l(k_j)}\left(2 - \frac{\rho\tilde{C}_l(k_j)}{k_j - \rho\tilde{C}_l(k_j)}\right) \times \mathcal{C}_{l\lambda;ij} \ , \tag{A9}$$

with $i,j = 1,\ldots,M$. Once the procedure converges one must calculate the remaining values of $\tilde{\Gamma}_l(k_j)$ for $j = M+1,\ldots,N$. This is done by direct substitution in the OZ relation (A1). Then $\tilde{\Gamma}_l(k)$ is transformed back to real space, and a new estimate of $\Gamma(r_i)$ is evaluated by using Broyles procedure [38], which makes the method more robust, i.e.,

$$\Gamma_l^{(s+1)}(r_i) = \alpha\Gamma_l^{(s+1)}(r_i) + (1-\alpha)\Gamma_l^{(s)}(r_i) \ . \tag{A10}$$

A value of $\alpha \approx 0.5$ seems optimum. Convergence is further accelerated by implementing a procedure that forces α to approach one when getting close to the final solution [14].

[1] G. Bush and H.J. Guentherodt, Phys. Lett. **27A**, 110 (1968); *Phase Transitions* (Interscience, New York, 1971), p. 179.
[2] B. Kraeft and H. Alexander, Phys. Konden. Mater. **16**, 281 (1973).
[3] J.S. Høye and G. Stell, Phys. Rev. Lett. **36**, 1569 (1976).
[4] P.T. Cummings and G. Stell, Mol. Phys. **43**, 1267 (1981).
[5] E. Martina and G. Stell, J. Stat. Phys. **27**, 407 (1982).
[6] L. Feijoo, C.W. Woo, and V.T. Rajan, Phys. Rev. B **22**, 2404 (1980).
[7] P.C. Hemmer and D. Imbro, Phys. Rev. A **16**, 380 (1977).
[8] D. Marx, P. Nielaba, and K. Binder, Phys. Rev. Lett. **67**, 3124 (1991).
[9] E. Lomba, J.J. Weis, and G. Stell (unpublished).
[10] F. Lado, S.M. Foiles, and N.W. Ashcroft, Phys. Rev. A **28**, 2374 (1983).
[11] F. Lado, Mol. Phys. **47**, 283 (1982).
[12] A.Z. Panagiotopoulos, Mol. Phys. **61**, 813 (1987).
[13] J.J. Weis, D. Levesque, and G.J. Zarragoicoechea, Phys. Rev. Lett. **69**, 913 (1992).
[14] E. Lomba, Mol. Phys. **68**, 122 (1989).
[15] N.W. Ashcroft, Nature **365**, 387 (1993).
[16] E. Lomba and N.G. Almarza, J. Chem. Phys. (to be published).
[17] L. Blum and A.J. Torruella, J. Chem. Phys. **56**, 303 (1972).
[18] L. Verlet and J.J. Weis, Phys. Rev. A **5**, 939 (1972); D. Henderson and E.W. Grundke, J. Chem. Phys. **63**, 601 (1975).
[19] M. Kinoshita and M. Harada, Mol. Phys. **74**, 443 (1991).
[20] G. Zerah and J.P. Hansen, J. Chem. Phys. **84**, 2336 (1986).
[21] S.M. Foiles, N.W. Ashcroft, and L. Reatto, J. Chem. Phys. **80**, 4441 (1984).
[22] E. Lomba, M. Alvarez, G. Stell, and J.A. Anta, J. Chem. Phys. **97**, 4349 (1992).
[23] Lifshitz and Pitaeevskii, *Electrodynamics of Continuous Media* (Pergamon, Oxford, 1982).
[24] F. Lado, Mol. Phys. **47**, 313 (1982).
[25] J.S. Høye and G. Stell, Mol. Phys. **32**, 195 (1976).
[26] J.S. Høye and G. Stell, Mol. Phys. **32**, 209 (1976).
[27] G.S. Rushbrooke, G. Stell, and J.S. Høye, Mol. Phys. **26**, 1119 (1973).
[28] A. Z. Panagiotopoulos, Mol. Sim. **9**, 1 (1992).
[29] R.F. Craknell, D. Nicholson, and N.G. Parsonage, Mol. Phys. **71**, 931 (1990).
[30] M.P. Allen and D. Tildesley, *Computer Simulation of Liquids* (Clarendon Press, Oxford, 1987).
[31] L. Belloni, J. Chem. Phys. **98**, 8080 (1993).
[32] J.S. Høye, E. Lomba, and G. Stell, Mol. Phys. **79**, 523 (1993).
[33] P.T. Cummings and G. Stell, J. Chem. Phys. **78**, 1917 (1983).
[34] J.A. Anta, E. Lomba, and M. Lombardero, Phys. Rev. E **49**, 402 (1994).
[35] H. Müller-Krumbhaar and K. Binder, Z. Phys. **254**, 269 (1972).
[36] Ch. Holm and W. Janke, Phys. Rev. B **48**, 936 (1993); K. Chen, A. M. Ferrenberg, and D.P. Landau, Phys. Rev. B **48**, 3249 (1993).
[37] S. Labik, A. Malijevsky, and P. Vonka, Mol. Phys. **56**, 709 (1985).
[38] A.A. Broyles, J. Chem. Phys. **33**, 456 (1960).